

JAAS

Accepted Manuscript

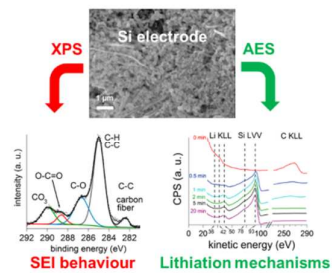


This is an *Accepted Manuscript*, which has been through the Royal Society of Chemistry peer review process and has been accepted for publication.

Accepted Manuscripts are published online shortly after acceptance, before technical editing, formatting and proof reading. Using this free service, authors can make their results available to the community, in citable form, before we publish the edited article. We will replace this *Accepted Manuscript* with the edited and formatted *Advance Article* as soon as it is available.

You can find more information about *Accepted Manuscripts* in the [Information for Authors](#).

Please note that technical editing may introduce minor changes to the text and/or graphics, which may alter content. The journal's standard [Terms & Conditions](#) and the [Ethical guidelines](#) still apply. In no event shall the Royal Society of Chemistry be held responsible for any errors or omissions in this *Accepted Manuscript* or any consequences arising from the use of any information it contains.



TOC Figure

By analyzing Si anodes using XPS and AES, both the SEI behaviour and the lithiation mechanisms are studied upon cycling.

Cite this: DOI: 10.1039/c0xx00000x

www.rsc.org/xxxxxx

ARTICLE TYPE

An XPS/AES comparative study of the surface behaviour of nano silicon anodes for Li-ion batteries

Etienne Radvanyi, Eric De Vito, Willy Porcher and Séverine Jouanneau Si Larbi*

Received (in XXX, XXX) Xth XXXXXXXXXX 20XX, Accepted Xth XXXXXXXXXX 20XX

DOI: 10.1039/b000000x

In this paper, the surface of composite electrodes made of nano silicon is studied by using two techniques of surface characterization: X-ray Photoelectron Spectroscopy (XPS) and Auger Electron Spectroscopy (AES). Several electrodes were analyzed at different States Of Charge (SOC) during the first electrochemical cycle. Firstly, the Solid Electrolyte Interphase (SEI) as well as the Si oxides present at the particles surface was thoroughly investigated. The behaviour of the SEI is close to that which forms on graphite: (i) its composition is similar and (ii) its thickness is greater at the lithiated state. Besides, our AES analyses carried out at the end of the first electrochemical cycle demonstrate that this behaviour strongly depends on the material it forms on: active material or conductive agent. Concerning SiO₂, which is initially present at the Si particles' surface, it is reduced irreversibly during the first lithiation. Simultaneously, our results clearly show the formation of Li₂O and Li_xSiO_y; these species are still observed during the aging of the electrode and systematically react at each cycle. Secondly, by using AES combined with a technique of sputtering, the first lithium insertion and the associated Li_xSi alloys were studied: several Si particles were investigated individually with respect to their electrode environment. After a capacity of 360 mAh.g⁻¹, the estimated Li concentration is different from a Si particle to another indicating that the first lithiation is a strongly heterogeneous process.

1. Introduction

In the past two decades, the demand for high-capacity Lithium-Ion Batteries (LIBs) for portable electronics, hybrid electric vehicles, and large scale energy storage has stimulated the research for new electrode materials¹⁻³. Metals and semi-metals that can electrochemically form alloys with lithium represent a relevant alternative to carbonaceous anodes^{4,5}. Silicon is considered as one of the leading candidates: the fully lithiated state of silicon at room temperature is Li₁₅Si₄ which corresponds to a capacity of 3580 mAh.g⁻¹, ten times larger than that of graphite⁶. Nevertheless, silicon undergoes huge volume changes upon alloying and dealloying with lithium: up to +300% compared to the initial volume for a full lithiation⁷. These volume changes are responsible for strong mechanical strains inside the silicon particles and subsequent loss of electrical contacts between the active material, the conductive matrix and the current collector resulting in poor cyclability for Si based electrodes⁸. To improve these electrochemical performances, many studies concerning the silicon material itself^{5,9,10}, the binder¹¹⁻¹³, or the formulation^{14,15} have been carried out. As an example, it has been shown that the use of silicon nanoparticles which better accommodate volume expansion¹⁶⁻²⁰, very much increases Si electrodes cyclability. Whatever the preferred solution, cycling performances of these electrodes, particularly in terms of coulombic efficiency remain so far unsatisfactory for a use in

practical LIBs.

One of the strong limitations has been recognized to be directly linked to electrode/electrolyte interfaces²¹⁻²⁴. Upon cycling, the electrolyte standardly made of LiPF₆ dissolved in carbonates is reduced and the resulting reduction products constitute a Solid Electrolyte Interphase (SEI) at the Si electrode surface^{23,25-28}. By using X-ray Photoelectron Spectroscopy (XPS), SEI composition which forms on Si electrodes has been found to be similar with that observed on graphite: it is mainly made of lithium alkyl carbonates, lithium carbonates, and lithium inorganic salts^{22,23,25-28}. Nevertheless, volume changes of Si particles can cause an important instability of this SEI. At each cycle, SEI reconstruction may consume lithium, electrolyte components, and electrons and consequently contribute to the irreversible capacity. The behaviour of this SEI upon cycling appears then as one of the key parameters governing the electrochemical performances of Si electrodes.

Interfacial chemistry of Si electrodes also concerns the study of the native Si oxides, especially SiO₂, present at the particles surface. Their behaviour and role are not well understood yet. According to Saint *et al*²⁹, the chances of the SiO₂ being reduced during the first lithiation following the reaction $SiO_2 + 4 Li \rightarrow Si + 2 Li_2O$ are extremely slim. On the contrary, Lee *et al*³⁰ showed, by using electrochemical impedance spectroscopy, that the native surface (SiO₂ and Si-OH) covering the Si electrode is destroyed at the beginning of the first lithiation. Finally, different

studies, by using XPS or Nuclear Magnetic Resonance, observed the reduction of SiO₂ upon cycling resulting in the formation of a supplemental phase attributed to Li₄SiO₄^{26,31} or Li₂Si₂O₅³². In addition, the impact of SiO₂ on the electrochemical performances of the electrodes has not been clearly identified^{33,34}.

In the present work, the surface of standard electrodes made of nano silicon is analyzed by using two techniques of surface characterization: XPS and Auger Electron Spectroscopy (AES). The literature concerning AES in the battery research field is quite rare³⁵⁻³⁹. However, by using this technique, our group showed recently the possibility to study lithiation mechanisms of micronic silicon occurring at the particle scale⁴⁰. In this work, the behaviour of Si electrodes surface is analyzed at different stages of the first lithiation/delithiation and during the following cycles; the interest and the potential complementarity of these two techniques of surface characterization for the study of nano silicon based electrodes are investigated and discussed.

2. Experimental Section

2.1 References samples

Thin films of Si and SiO₂ were used as reference samples. They were obtained following the smart cut process from SOITEC®. This process is based on a thermal activation *via* ion implementation and allows slicing wafers⁴¹.

2.2 Electrochemistry

A Si based slurry made of an aqueous mixture of nano silicon (65 wt %), carbon fibers (25 wt %), and Carboxy Methyl Cellulose (CMC) (10 wt %, M_w = 250 kg. mol⁻¹, D.S. = 0.7) was coated on a copper foil current collector. The loading of the electrode was 2 mg of Si by cm². Electrodes were then cut into 14 mm diameter disk shape, dried 48 h and moved into an argon-filled glove box. CR2032 coin cells were assembled using a lithium metal foil as the counter electrode, a Celgard® 2400 separator, a Viledon® propylene foil wetted by a liquid electrolyte (1M LiPF₆ in ethylene carbonate (EC): diethyl carbonate (DEC) (wt % of 1:1)) and a working electrode.

Galvanostatic charges and discharges were carried out with a current density of 0.3 mA.cm⁻² (corresponding to a C/20 rate based on a 3600 mAh.g⁻¹ capacity) at 25°C using a battery tester (Arbin®). The cut-off potentials of charge and discharge were respectively 1.2 and 0.005 V vs Li⁺/Li.

After cycling, the cells were relaxed until the derivation of the potential was inferior to 1 mV.h⁻¹. Si electrodes were then removed from the coin cells in the glove box and washed twice with dimethyl carbonate.

2.3 XPS characterization

Electrodes were transferred directly from the glove box to the XPS Fast Entry Lock (FEL) room using a sealed transfer vessel to avoid exposure to air. XPS measurements were carried out with an Omicron MXPS spectrometer using a focused monochromatized Al K α radiation (h ν = 1486.6 eV). The pass energy was set to 20 eV allowing an energy resolution of approximately 400 meV. No charge neutralization was used. The binding energy scale was calibrated from the hydrocarbon C 1s at 285 eV.

2.4 AES characterization

The samples were transferred from the glove box to the AES FEL using a sealed transfer vessel to avoid exposure to air. Auger measurements were achieved with a Physical Electronics 700Xi scanning Auger nanoprobe. The analyses were done at 5 kV / 5 nA. Spatial resolution as low as 20 nm can be reached while maintaining an energy resolution of 0.5%. SEM images were acquired by using a scintillator as the secondary electron detector. The analyses of the electrodes were carried out on an area of 100 x 100 μ m². AES depth profiles were obtained by using argon ion sputtering (1 keV / 1 μ A) with a tilt of the samples of 30°. During sputtering, Zalar rotation with a speed of one rotation per min was systematically used. Auger data were analyzed by using Multipak software. AES intensities correspond to the peak-to-peak height of the derivative spectra.

3. Results

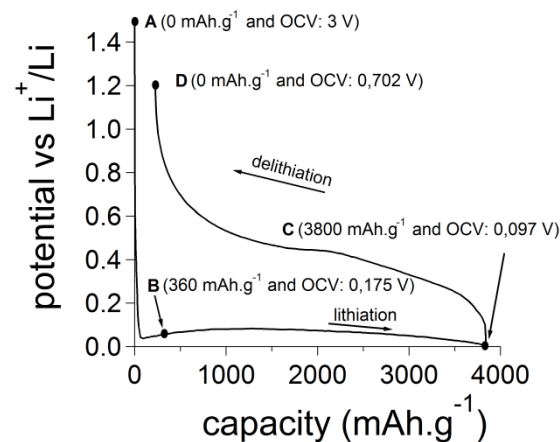


Fig. 1 First lithiation/delithiation cycle of the Si electrode vs Li metal cell between 0.005 V and 1.2 V at C/20 rate. The samples analyzed by XPS and AES are highlighted by black points; for each electrode, the capacity and the Open Circuit Voltage (OCV), *i. e.* the potential measured after relaxation, are indicated.

The first lithiation/delithiation (until reaching respectively 0.005 V and 1.2 V at C/20 rate) of an electrochemical cell built with the Si electrode vs metallic lithium is shown in Figure 1. The lithiation curve exhibits a plateau at 0.08 V which is in good agreement with previous results obtained on Si particles⁸. At the end of lithiation, the capacity is equal to 3800 mAh.g⁻¹, slightly superior to 3580 mAh.g⁻¹, corresponding to the formation of Li₁₅Si₄. It could be easily explained with the consumption of electrons, under 1 V, to reduce the electrolyte and form the SEI (this step is highlighted Figure S1). Upon delithiation, a capacity of 3500 mAh.g⁻¹ is restored. The electrochemical steps A, B, C, and D, indicated by black points with the associated capacities, represent the samples analyzed by XPS and AES. For each electrode, the Open Circuit Voltage (OCV), which is here the potential obtained after relaxation, corresponding to a derivation of the potential inferior to 1 mV.h⁻¹, is also reported. Thus, (i) electrode A is the pristine sample, (ii) electrode B corresponds to the beginning of the lithiation, (iii) electrode C can be associated with the end of the lithiation process, and (iv) electrode D can be related to the end of the delithiation step.

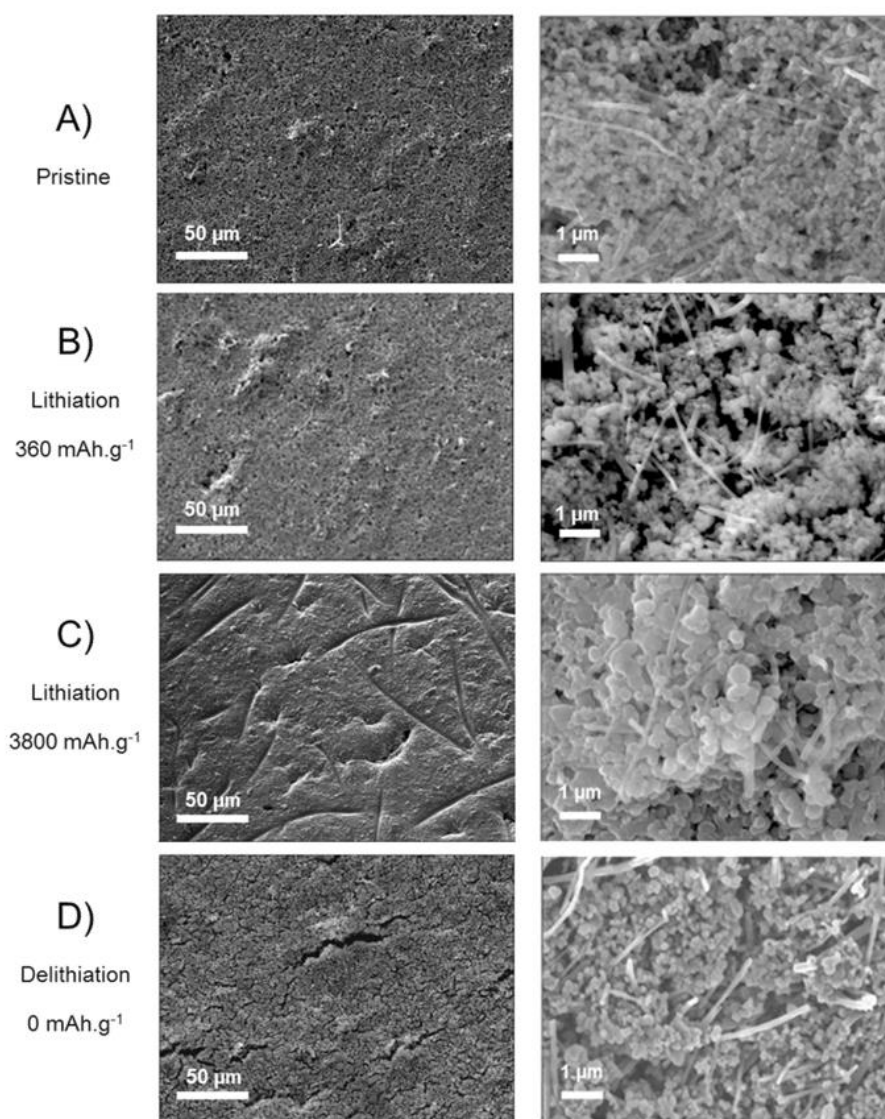


Fig. 2 SEM images (50 μm and 1 μm scales) of the Si electrodes: A) pristine electrode, B) after a capacity of 360 mAh.g^{-1} , C) after a capacity of 3800 mAh.g^{-1} , and D) after a complete electrochemical cycle.

5 Figure 2 shows the morphological changes undergone by the Si
 6 electrode upon lithiation and delithiation. According to the
 7 Scanning Electron Microscopy (SEM) images of the pristine
 8 electrode A), silicon particles are nanometric, their average
 9 diameter is around 200 nm; carbon fibers are 5 to 10 μm long
 10 with a diameter close to 150 nm.

11 There is no visible change after a lithiation of 360 mAh.g^{-1}
 12 (electrode B). However, after a full lithiation, it appears that the
 13 alloying process between Li and Si results in a huge volume
 14 expansion of the particles (1 μm image of electrode C).
 15 Interestingly, the apparent diameter of the lithiated particles is
 16 close to 500 nm, corresponding to an initial volume multiplied by
 17 around 15, almost four times the expected value. This apparent
 18 volume increase of the Si particles can be explained by (i) the
 19 formation of a thick SEI at the electrode surface during lithiation

20 and/or (ii) a kind of sintering phenomenon between neighbouring
 21 particles, already observed by using Transmission Electron
 22 Microscopy (TEM)⁴². Prints of fibers are clearly visible at the
 23 electrode surface (50 μm image of electrode C). One can assume
 24 that they have been left by the polypropylene separator pressed at
 25 the electrode surface during lithium insertion: lithiation leads to
 26 an increase of the particles volume but also of the electrode
 27 thickness.

28 Upon delithiation, the removal of lithium results in the formation
 29 of cracks (50 μm image of electrode D) inside the electrode but
 30 the Si particles recover their initial morphology which is in good
 31 agreement with previous results obtained on Si nanoparticles (1
 32 μm image). The prints of the separator fibers are not visible any
 33 more indicating that the electrode thickness has decreased.

Cite this: DOI: 10.1039/c0xx00000x

www.rsc.org/xxxxxx

ARTICLE TYPE

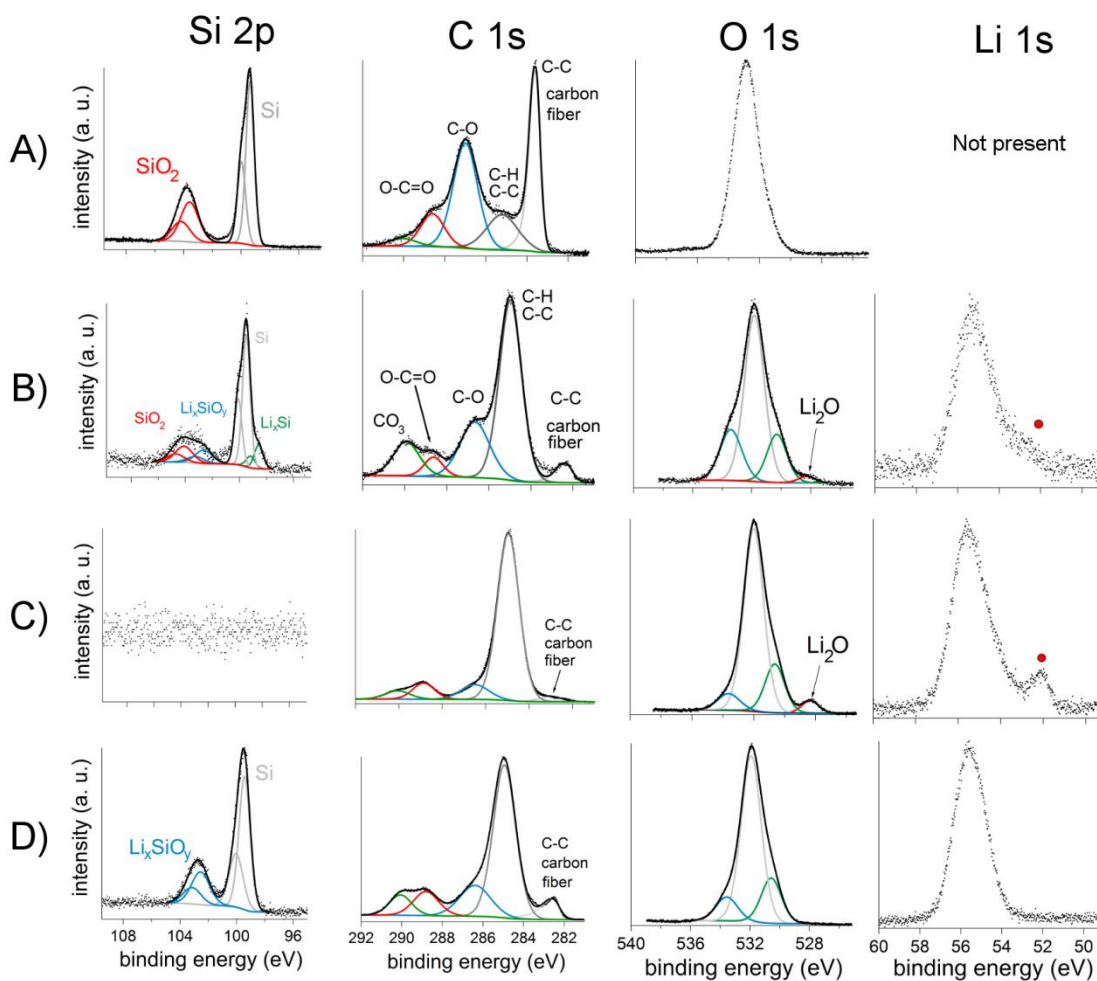


Fig. 3 XPS spectra (Si 2p, C 1s, O 1s, and Li 1s core peaks) obtained at the surface of the Si electrodes: A) pristine electrode, B) after a capacity of 360 mAh.g⁻¹, C) after a capacity of 3800 mAh.g⁻¹, and D) after a complete electrochemical cycle.

Cite this: DOI: 10.1039/c0xx00000x

www.rsc.org/xxxxxx

ARTICLE TYPE

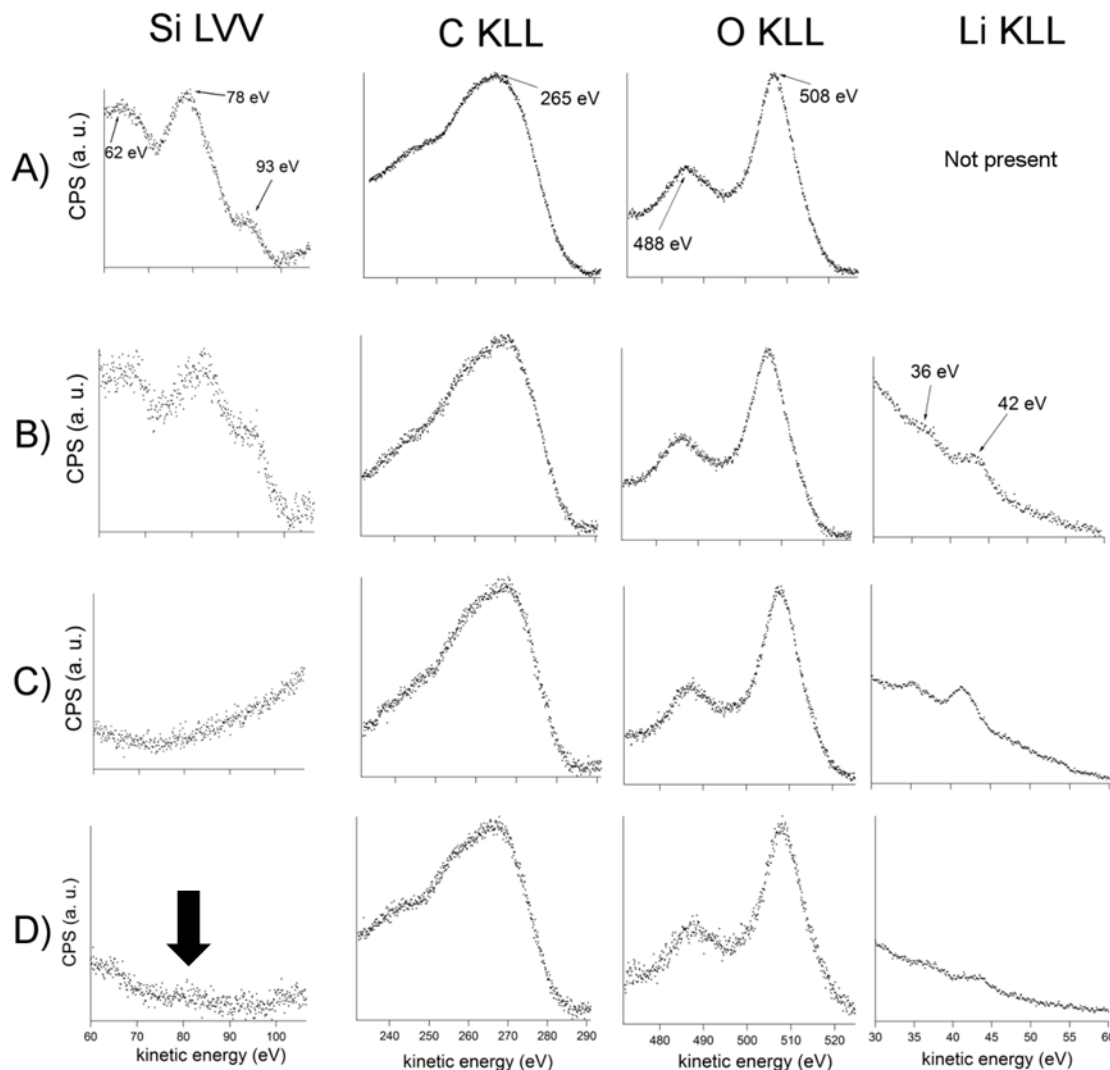


Fig. 4 Auger spectra (Si LVV, C KLL, O KLL, and Li KLL transitions) obtained at the surface of the Si electrodes: A) pristine electrode, B) after a capacity of 360 mAh.g⁻¹, C) after a capacity of 3800 mAh.g⁻¹, and D) after a complete electrochemical cycle.

3.1 Electrode A (pristine)

Figures 3A) and 4A) show the spectra corresponding respectively to Si 2p, C 1s, O 1s core peaks and Si LVV, C KLL, and O KLL Auger transitions at the surface of the pristine electrode. Si, C, and O are identified with both techniques. The XPS data presented here are in good agreement with the results obtained by Philippe *et al.*²⁶. Concerning silicon, the spectrum displays a first Si 2p peak (composed of 2p_{3/2} and 2p_{1/2} due to spin-orbit coupling) assigned to bulk silicon (~99.5 eV in grey) and another one assigned to surface oxide SiO₂ (~103.8 eV in red). Some other Si oxides may also be present (binding energy at around

~102 eV) but in very small quantity. C 1s spectrum shows several components. The narrow peak at ~283.8 eV corresponds to C-C bonds associated here with the carbon fibers. The two peaks at ~287 and ~288.5 eV (respectively blue and red) can be attributed to C-O and O=C-O environments of carbon atoms in the CMC binder. Finally, the component at 285 eV is assigned to hydrocarbon surface contamination. O 1s spectrum is composed of one major component at ~532.5 eV associated with O environments in the CMC binder and in the native oxide SiO₂.

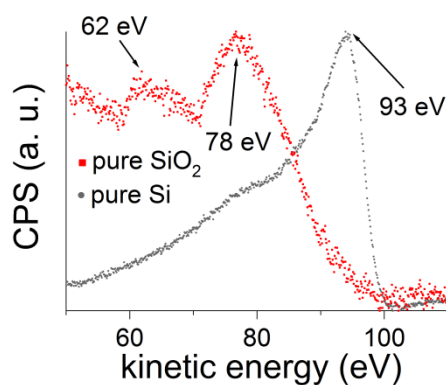


Fig. 5 Auger spectra corresponding to Si LVV transition obtained for pure SiO₂ and pure Si.

As far as we know, there has been no published AES analysis of electrodes made of nano silicon. Figure 5 shows the AES spectra obtained at the surface of pure SiO₂ and pure Si. Two peaks at 62 and 78 eV are observed for SiO₂. One main peak at 93 eV is obtained for Si. These results are in good agreement with AES analyses obtained previously^{43,44}. Figure 4A) shows the presence of these 3 peaks for the Si LVV transition. It is consistent with the XPS results: the analyzed electrodes contain Si particles covered by a native oxide. Concerning C and O, the interpretation of the peaks is much more difficult. Few references are available in the literature. Among them, AES studies carried out on graphite report a main peak at 269 eV for C KLL^{45,46}; Zhu and Cao⁴³ show a main peak at 502.1 eV for O KLL in a SiO₂ environment. However, the separation of the different environments of O and C is very challenging, as it has been reported previously⁴⁷.

If chemical information brought by XPS is much more abundant especially for carbon, XPS and AES analyses of the pristine electrode lead to similar conclusions: (i) Si, C, and O are detected at the electrode surface and (ii) Si particles are covered by a SiO₂ layer. As bulk silicon is detected in both analyses, a maximal thickness of this layer can be calculated by using QUASES@ simulation software developed by Tougaard⁴⁸. In SiO₂, The Inelastic Mean Free Paths (IMFPs) of electrons with a kinetic energy of 1386 eV (photoelectrons emitted from Si 2p) and 100 eV (Auger electrons from Si LVV) are found to be respectively 38 Å and 8 Å, leading to a maximal thickness of SiO₂ of around 2.4 nm.

3.2 Electrode B (after a capacity of 360 mAh.g⁻¹)

Figures 3B) and 4B) show the spectra corresponding respectively to Si 2p, C 1s, O 1s, Li 1s core peaks and Si LVV, C KLL, O KLL, and Li KLL Auger transitions at the surface of electrode B, after a capacity of 360 mAh.g⁻¹. The elements Si, C, O, Li, F, and P are detected (XPS and AES spectra corresponding to F and P are represented in the supplemental information Figure S2) by using both techniques. The presence of C, O, Li, F, and P can be directly related to the reduction of the electrolyte and the formation of the SEI at the electrode surface. These phenomena have been widely reported to occur below 1 V when the electrolyte is composed of LiPF₆ dissolved in carbonates⁴⁹.

The C 1s signal of carbon fibers is detected but the relative intensity of this contribution is much lower than that of the

pristine electrode, confirming that a new layer has formed at the electrode surface. New C environments are revealed, particularly CO₃ at ~290 eV which can be attributed to new carbonaceous species including Li₂CO₃ and lithium alkyl carbonates, actually reported as SEI components for graphite electrodes⁴⁹. One major peak is observed for O 1s at ~532 eV, in good agreement with carbonates and organic species⁵⁰. Interestingly, a peak is detected at ~528 eV, which can be associated with Li₂O^{26,51}. The peak at ~52 eV highlighted by a red spot observed on Li 1s spectrum may also be related to the presence of Li₂O. However, as there are only few references in the literature⁵¹⁻⁵³, this attribution is discussed later on. In addition, F 1s (Figure S2) shows two components which can correspond to (i) LiPF₆ salt (at ~687.5 eV in red) remaining at the electrode surface and (ii) LiF (at ~685.5 eV in blue) resulting from the reduction of the salt anion PF₆⁻. Si 2p shows 4 components. A first contribution is found at 98.5 eV which can be attributed to Li_xSi^{26,54}. The detection of this phase indicates that lithiation has already started after a capacity of 360 mAh.g⁻¹. A second peak at ~99.5 eV is observed suggesting that there is still unreacted bulk silicon at the electrode surface. Two oxidized forms of Si are detected as well respectively at ~104 eV and ~102.5 eV. They can be attributed respectively to the SiO₂ found initially and to a new phase Li_xSiO_y already observed at silicon electrodes surface^{26,27,33,55}.

Compared to the pristine electrode, Si LVV spectrum has changed with a decrease of the signal associated with SiO₂ at ~78 eV and an increase of the signal at 93 eV corresponding to bulk silicon or a Li_xSi alloy, in good agreement with XPS data. Two peaks are detected for Li KLL spectrum at 36 and 42 eV. These kinetic energies have been reported in previous works and associated with Li in an oxidized form^{37,40}; they can be related to the presence of Li compounds including Li₂CO₃ and lithium alkyl carbonates at the electrode surface. C KLL and O KLL spectra are very close to the ones obtained for the pristine electrode. F and P are detected as well which is consistent with the presence of LiF and LiPF₆ at the electrode surface. In order to try to resolve the AES spectra and identify the different components especially for C KLL, O KLL, and F KLL, we analyzed reference compounds including Li₂CO₃ and LiF. Unfortunately, despite several attempts by using Ar⁺ ion gun as a neutralizer gun (E_{Ar^+} ~70 eV) or mixing the products with highly divided carbon, we have not been able so far to get valuable AES data.

In a previous study we obtained interesting information concerning the process of the first Li insertion in Si micronic particles by using AES combined with Ar⁺ sputtering⁴⁰. As the size of the active material may impact the lithiation mechanisms, the same kind of measurements are carried out here. The high spatial resolution of the Auger spectrometer⁵⁶⁻⁵⁸ allows the surface behaviour of different silicon particles in their electrode environment to be studied separately. A complete study of one silicon particle is detailed thereafter.

Figure 6 shows a SEM image of the investigated particle. Depth profiling has been achieved inside this silicon particle: at regular sputtering intervals, Auger analyses corresponding to Li KLL, Si LVV, and C KLL Auger transitions were performed. All the analyses are carried out on the same area in the center of the particle. In order to minimize shadow effects and to improve sputtering homogeneity, sputtering was combined with Zalar

rotation. This technique is particularly interesting when the surface of the analyzed sample is rough, as in the case of these electrodes. Figure 7 shows the evolution with sputter time of the spectra obtained. The Auger analyses obtained before sputtering are similar to the ones shown in Figure 4B). As soon as sputtering starts, Li KLL energy peaks at 36 and 42 eV disappear and a new peak is observed at 50 eV. The intensity of the C KLL peak decreases dramatically and Si LVV transition is revealed at 93 eV. Figure 8 shows the evolution with sputter time of the AES intensities of Li KLL (I_{Li}), Si LVV (I_{Si}), and C KLL (I_C); I_{Li} and I_{Si} are associated respectively with the peaks at 50 and 93 eV. During the first minute of sputtering, I_C actually decreases until reaching a very low value corresponding to a ratio I_C/I_{Si} lower than 0.03. In the same time, I_{Li} and I_{Si} increase before stabilizing; the ratio I_{Li}/I_{Si} is then equal to 0.21 ± 0.03 . Sputtering can hardly be carried out over 20 min before destroying the particle (Figure S3). By analyzing well-known Li-Si alloys, we calculated several Alloy Reference Relative Sensitivity Factors⁴⁰. Based on $R_{Li}^{Li_{15}Si_4}$, a ratio of 0.21 corresponds to a composition of $Li_{1.6}Si$. Figure 9 shows the evolution with sputter time of Li_xSi compositions obtained for 3 silicon particles, particle 1 is the one shown in Figure 6. A constant ratio Li-Si is observed inside all the investigated particles. Interestingly, this ratio varies from a particle to another.

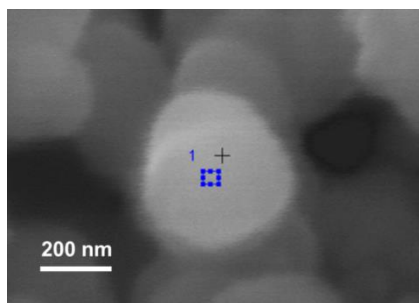


Fig. 6 SEM image of a Si particle from the surface of electrode B, after a capacity of 360 mAh.g^{-1} . AES analyses were carried out on the area represented by the blue square.

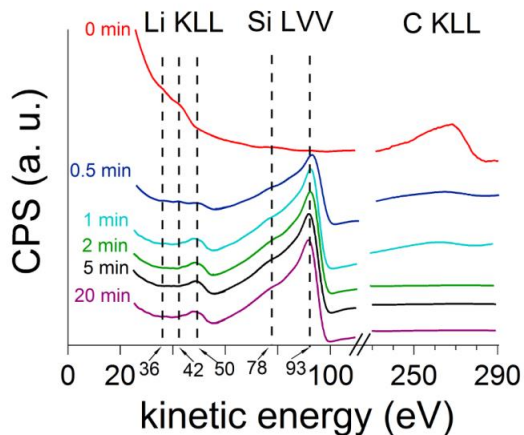


Fig. 7 Evolution with sputter time of AES spectra for Li KLL, Si LVV, and C KLL obtained at the surface of the Si particle shown in Figure 6.

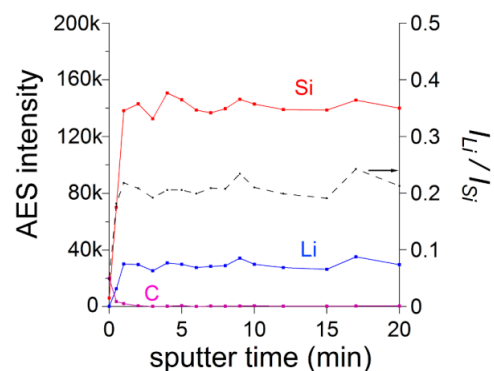


Fig. 8 Evolution with sputter time of I_{Li} , I_{Si} , I_C , and the ratio I_{Li}/I_{Si} obtained at the surface of the Si particle shown in Figure 6.

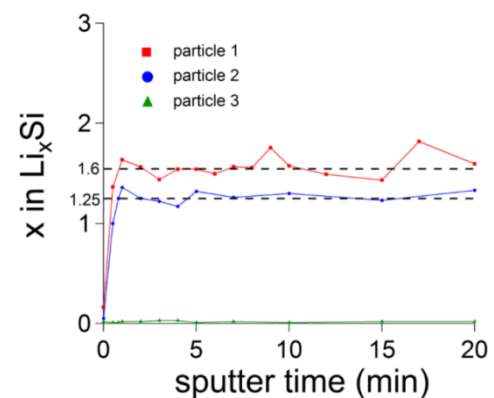


Fig. 9 Evolution of the Li-Si compositions with sputter time obtained for three particles from electrode B, after a capacity of 360 mAh.g^{-1} .

3.3 Electrode C (after a capacity of 3800 mAh.g^{-1})

Figures 3C) and 4C) show the spectra corresponding respectively to Si 2p, C 1s, O 1s, Li 1s core peaks and Si LVV, C KLL, O KLL, and Li KLL Auger transitions at the surface of electrode C, after a capacity of 3800 mAh.g^{-1} . Si is not observed by using both XPS and AES indicating that the SEI layer has become thicker with lithiation. Again, based on Quases® software, a minimal thickness of the SEI at Si particles surface can be determined. For a large range of organic materials, IMFPs of electrons with a kinetic energy of 1386 eV (photoelectrons emitted from Si 2p) and 100 eV (Auger electrons from Si LVV) are found to be respectively 40 and 7 Å, leading to a minimal thickness of around 12 nm. The increase of this thickness is confirmed by the decrease of the signal associated with the carbon fibers on C 1s spectrum compared to Figure 3B). The general shape of C 1s, O 1s, and Li 1s spectra is similar to the one obtained from electrode B. Only small fluctuations are observed suggesting that the SEI composition is rather stable upon lithiation. However, the increase of the peak attributed to Li_2O both on O 1s spectrum at $\sim 528 \text{ eV}$ as well as on Li 1s spectrum at $\sim 52 \text{ eV}$ is clearly visible. The Auger spectra are similar to the ones obtained for electrode B. According to the SEM images (Figure 2), the volume and the surface of the active material undergo important variations upon lithiation; on the contrary, the carbon fibers are supposed to be rather stable. It may induce differences concerning the behaviour of the SEI which forms at the surface of these materials. Again, taking advantage of AES spatial resolution⁵⁶⁻⁵⁸, Auger analyses

were carried out on a carbon fiber and on a Li-Si particle (Figure S4). No difference was observed.

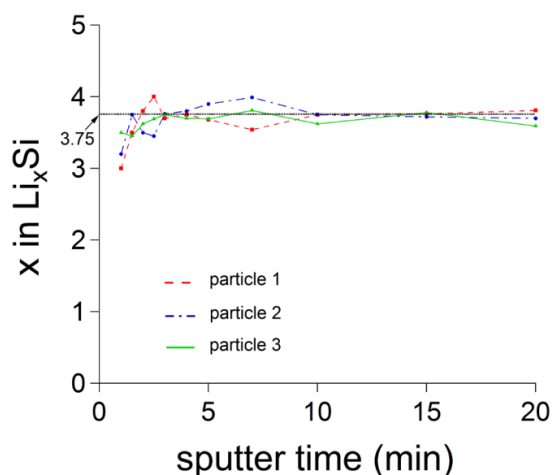


Fig. 10 Evolution of the Li-Si compositions with sputter time obtained for 3 particles from electrode C, after a capacity of 3800 mAh.g^{-1} .

In addition, several Si particles from the surface of electrode C have been investigated with AES and Ar^+ sputtering following the same procedure described previously. Figure 10 shows the evolution with sputter time of Li_xSi compositions obtained for 3 silicon particles. After removing the SEI, which corresponds to a sputter time of approximately 2 min, the composition inside all the particles, calculated by using $R_{\text{Li}}^{\text{Li}_{15}\text{Si}_4}$, is found to be close to $\text{Li}_{3.75}\text{Si}$ confirming that a full lithiation has been actually achieved.

3.4 Electrode D (after a complete electrochemical cycle)

Figures 3D) and 4D) show the spectra corresponding respectively to Si 2p, C 1s, O 1s, Li 1s core peaks and Si LVV, C KLL, O KLL, and Li KLL Auger transitions at the surface of electrode D, after a complete electrochemical cycle. A Si signal is observed on Si 2p spectrum indicating that SEI thickness has decreased compared to electrode C, associated with a full lithiated state. This result is confirmed with the increase of the signal associated with the carbon fibers on C 1s spectrum. The other components of C 1s spectrum are the same than as observed at the surface of electrodes B and C: CO_3 , $\text{O}=\text{C}-\text{O}$, $\text{C}-\text{O}$, $\text{C}-\text{C}$, and $\text{C}-\text{H}$. The major peak at $\sim 532 \text{ eV}$ corresponding to carbonates and organic species

is detected on O 1s spectrum. Li_2O is detected neither on O 1s nor on Li 1s spectrum. No change is observed on F 1s spectrum (Figure S5). The analysis of Si 2p spectrum reveals the presence of only two components: (i) a peak corresponding to bulk silicon at $\sim 99.5 \text{ eV}$ and (ii) a peak at $\sim 102.5 \text{ eV}$ corresponding to a Li_xSiO_y phase, as seen for electrode B. It is interesting to note that (i) SiO_2 is not seen at all and (ii) no peak at 98.5 eV is detected indicating that at the end of the delithiation, no Li remains alloyed with Si at the particles surface. Concerning the AES analyses, a weak peak is observed around 80 eV (shown with the arrow on Si LVV spectrum) indicating that a Si oxide is detected. It confirms a decrease of the SEI thickness, in good agreement with the XPS results. C KLL, O KLL, and Li KLL spectra are very close to the ones obtained for electrodes B and C. As done for electrode C, Auger analyses were carried out on a carbon fiber and on a Si particle. Figure 11 shows the analyzed zone (the blue square on the SEM image) and the spectrum associated with Li KLL transition for a) a Si particle and b) a carbon fiber. Both spectra are different; Li signal is much more intense at the surface of the carbon fiber.

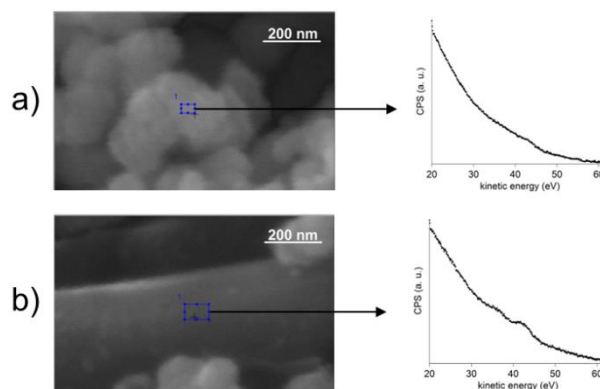


Fig. 11 SEM image and Li Auger spectrum at the surface of electrode D, after a complete electrochemical cycle a) for a silicon particle and b) for a carbon fiber. The Auger analyzed area is represented by a blue square on the SEM image.

To go further, we achieved AES mappings of another area of electrode D for two elements: lithium and silicon (Figure 12). A SEM image is also represented where several silicon particles and one carbon fiber are clearly visible. Li mapping confirms that Li is much more abundant at the surface of the carbon fibers.

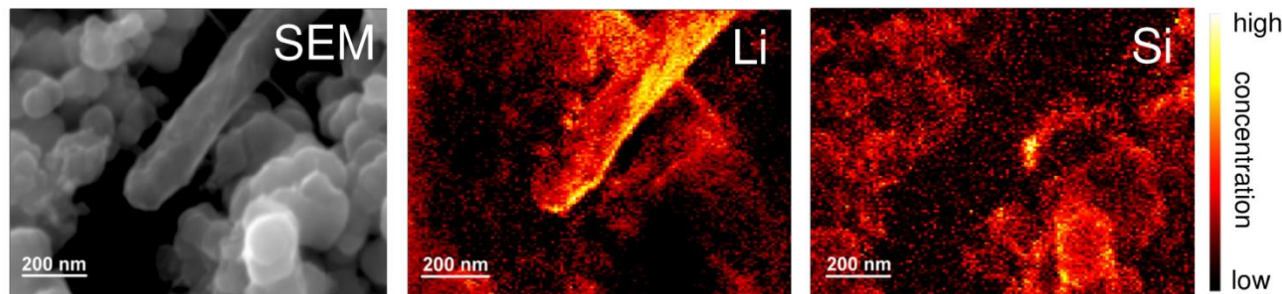


Fig. 12 SEM image and AES elemental mappings of Li and Si at the surface of electrode D, after a complete electrochemical cycle.

Cite this: DOI: 10.1039/c0xx00000x

www.rsc.org/xxxxxx

ARTICLE TYPE

In addition, following the same procedure described previously, several particles were investigated by using AES and Ar⁺ sputtering. The results are consistent with the XPS observations: no Li alloyed with Si was revealed inside all the investigated particles (around 10).

3.5 Following cycles

Figure 13 shows the spectra corresponding to Si 2p, O 1s, and Li 1s core peaks after 5 electrochemical cycles at the end of delithiation and lithiation. At the end of delithiation, Si is

detected. Again, Si 2p spectrum shows two components: the peak at ~99.5 eV corresponding to bulk silicon and the peak at ~102.5 eV associated with the Li_xSiO_y phase. The shape of O 1s and Li 1s spectra is very close to the one obtained from electrode D, at the end of the first delithiation. In particular, no Li₂O is detected. At the end of the fifth lithiation, no Si peak is detected probably again because of an increase of the SEI thickness and Li₂O is observed both on O 1s and Li 1s spectra.

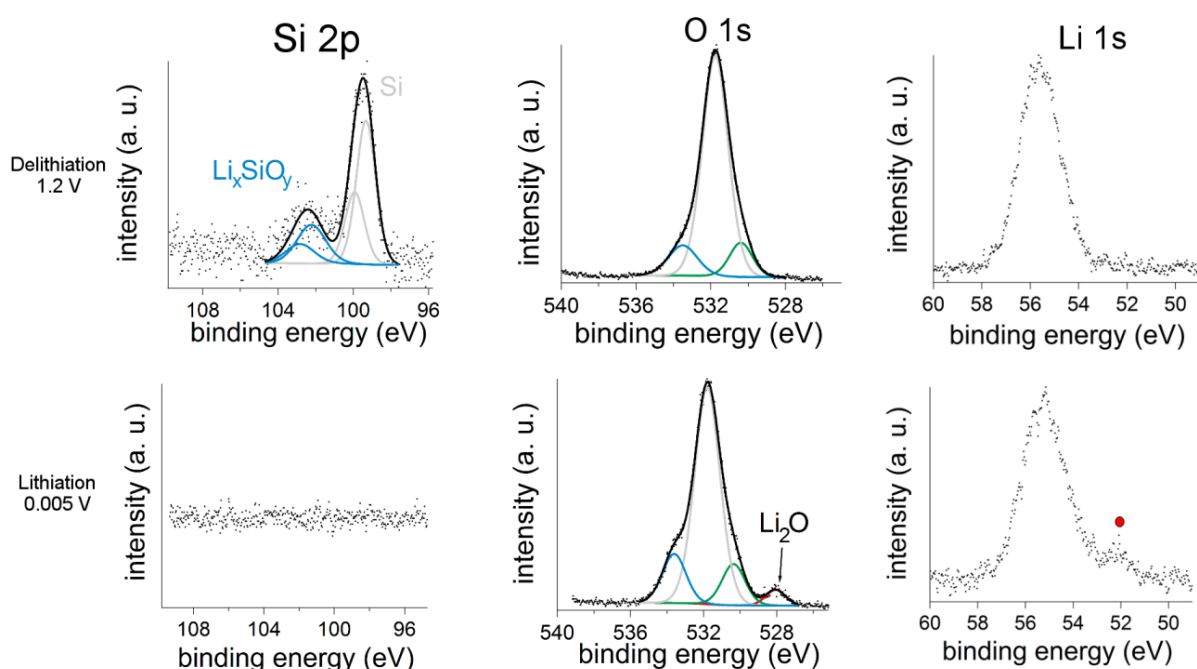


Fig. 13 XPS analyses obtained at the surface of the Si electrode during the fifth electrochemical cycle (i) after delithiation at 1.2 V and (ii) after lithiation at 0.005 V.

4. Discussion

Table 1 Elemental composition of the surface of the Si electrodes based on the XPS results. In addition SEI thickness estimations based on XPS and AES analyses have been calculated.

	Si	C	O	Na	Li	F	P	SEI thickness from XPS	SEI thickness from AES
Electrode A	27%	38%	27%	8%	Not present	Not present	Not present	Not present	Not present
Electrode B	5%	37%	21%	Not detected	32%	4%	1%	<12 nm	<2.4 nm
Electrode C	Not detected	49%	16%	Not detected	30%	4%	1%	>12 nm	>2.4 nm
Electrode D	3%	39%	20%	Not detected	31%	5%	2%	<12 nm	<2.4 nm

4.1 Behaviour of the SEI

After a capacity of 360 mAh.g⁻¹ (electrode B), the decrease of the XPS and AES signals associated with Si⁰ and the carbon fibers compared to the pristine electrode indicate the formation of a new layer at the electrode surface. This layer is made of Li, P, C, O, and F and can be identified to the SEI resulting from the electrolyte reduction. The binding energies from the XPS spectra are consistent with species already observed on graphite or silicon electrodes during cycling such as lithium carbonates, lithium alkyl carbonates and LiF^{22,26,27}. Table 1 shows the elemental composition of the electrodes surface obtained from the XPS analyses. In addition, a maximal or minimal thickness of the SEI has been estimated for each electrode. The calculations are simply based on the detection of Si as it is detailed in the previous section. Note that the calculation of the electrons IMFPs was based on a kinetic energy of 1386 eV for the XPS analyses (photoelectrons emitted from Si 2p) and 100 eV for the AES analyses (Auger electrons from Si LVV). These results show that (i) the composition and (ii) the thickness of the SEI depend on the SOC of the electrode. Thus, the thickness of the SEI varies from less than 3 nm at the delithiated state to more than 12 nm at a full lithiated state. This behaviour of the SEI is not specific to silicon electrodes and has already been observed for graphite and AlSb electrodes^{59,60}.

If further work needs to be carried out to deeply interpret the Auger spectra, it appears that AES allows studying the SEI with respect to its localization at the electrode surface. As illustrated by the lithium concentration detected on carbon fibers and Si particles at the end of the first electrochemical cycle (Figures 11 and 12), the SEI behaviour concerning its thickness and/or composition depends on the material it forms on. We assume that these results are directly related to the differences concerning the surface dynamic between the active material and the conductive additive.

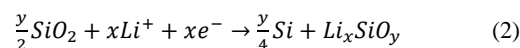
4.2 Evolution of the Si-containing phases

4.2.1 First lithiation

Before any cycling (Figure 3A), the peak at ~103.8 eV on Si 2p spectrum indicates the presence of a native oxide layer at the surface of the silicon particles. This layer can be identified to SiO₂. Si 2p spectrum from electrode B (Figure 3B)) shows a decrease of this signal and reveals a new contribution at 102.5 eV. The formation of a new component has already been observed in previous works and associated to the appearance of a Li_xSiO_y phase, as a consequence of the electrochemical reduction of SiO₂^{26,31-33,55}. We were not able to determine the exact composition of this Li_xSiO_y phase: according to the literature, a signal at ~102.5 eV can be associated with the presence of several products including Li₄SiO₄, Li₂Si₂O₅, or Si suboxides^{26,31-33}. Consequently, this new phase will be designated by the general formula Li_xSiO_y in the following discussion. The formation of Li_xSiO_y is concomitant to the appearance of signals which can be related to the presence of Li₂O at the electrode surface (Figure 3B)): (i) a peak at ~528 eV on O 1s spectrum and (ii) a peak at ~52 eV on Li 1s spectrum. The peak at 528 eV has been clearly reported several times as associated with Li₂O^{26,51,52,61}. As the binding energies corresponding to Li₂O for Li 1s are found in the

literature to vary from 53 to 55 eV^{51-53,61}, it was more difficult to attribute unequivocally the peak at 52 eV. However, firstly, this peak cannot be related to a Li_xSi phase. Indeed, the XPS results obtained on electrode C, after a full lithiation, show clearly a 52 eV peak on Li 1s spectrum and no peak is detected on Si 2p spectrum, whereas the Relative Sensitivity Factors of Li and Si are respectively 0.0568 and 0.817. Secondly, as the C-rate is low, it is hard to believe that Li metal was deposited at the electrode surface during cycling. Finally, Table 2 indicates the amounts of Li and O calculated from the peaks at 52 and 528 eV. Li₅₂ eV quantity is nearly twice the amount of O₅₂₈ eV, in good agreement with the composition of Li₂O.

These results suggest that during the first lithiation, SiO₂ is reduced to Si or Li_xSiO_y as follows:



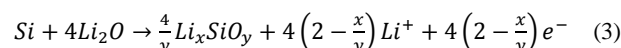
The increase of the signals associated with Li₂O on XPS spectra of Figure 3C) compared to Figure 3B) indicates that the reduction of SiO₂ continues with further lithiation.

Table 2 O and Li amounts based respectively on the 528 eV and on the 52 eV peaks from the XPS results.

	O in Li ₂ O	Li in Li ₂ O
Electrode A	Not present	Not present
Electrode B	1%	1.5%
Electrode C	1.5%	2.5%
Electrode D	Not detected	Not detected

4.2.2 First delithiation

The XPS analyses at the end of delithiation from electrode D (Figure 3D)) reveal the presence of Li_xSiO_y whereas Li₂O is detected neither on Li 1s nor on O 1s spectrum. Based on these observations, the following reaction can be proposed:



Moreover, contrary to what has been reported before²⁶, SiO₂ is not observed at the end of delithiation after reaching a potential of 1.2 V indicating that in our case, reactions (1) and (2) are not reversible.

4.2.3 Following cycles

The XPS results obtained after 5 electrochemical cycles (Figure 13) indicate that reaction (3) is reversible and happens at every cycle as a consequence of the electrochemical Li insertion/desinsertion. Besides, the complete and definitive reduction of the initial SiO₂ layer has a strong impact on the surface chemistry of the Si particles. Philippe *et al*^{26,27} reported the presence of some SiO₂ remaining at the particles surface after the first electrochemical cycle. In their case, by reacting with the LiPF₆ containing electrolyte, SiO₂ transforms into SiO_wF_z during cycling. According to the authors, the formation of this fluorinated phase at the extreme surface of the particles considerably deteriorates the interaction between Si and the CMC binder leading to a quick degradation of the electrode performances. In our case, no fluorinated species is observed

after 5 electrochemical cycles. These results lead us to the following conclusions: (i) as proposed by Philippe *et al*²⁷, SiO_wF_z formation comes from a reaction involving SiO₂ and (ii) it seems possible to avoid the formation of this fluorinated phase without changing the Li salt in the electrolyte⁶². Thus, the conditions to completely reduce the SiO₂ layer during cycling need to be deeper investigated. The following parameters should be probably looked at: the initial silicon material itself (size, morphology, surface chemistry, and nature of Si oxides) and the cycling conditions.

4.3 First lithiation process

The XPS results of electrode B with the presence of a peak at 98.5 eV on Si 2p spectrum indicates that lithiation has started after a capacity of 360 mAh.g⁻¹. It is in good agreement with the detection of Li alloyed with Si inside the particle shown in Figure 6. These last AES results suggest that Li concentration is constant inside the particle investigated. This Li distribution was quite unexpected at the particle scale during the first lithiation: firstly, our experiments on micronic silicon particles demonstrated the presence of at least 2 phases inside a single Si particle with a highly lithiated shell Li₃Si and a core of pure silicon⁴⁰; and secondly many studies of silicon nano particles notably by using *in situ* TEM show clearly a core-shell structure with an amorphous Li_xSi shell and a core of crystalline silicon inside⁶³. Several hypotheses can explain the results obtained in this work including (i) the spatial resolution of the technique has been reached, (ii) as the experiments carried out are *ex situ*, Li has diffused inside the whole nanoparticle while sputtering is performed, and (iii) the sputtering process as it is used here cannot clearly reveal different phases when their thickness is only a few dozens of nm. Identical measurements were carried out on other silicon particles of electrode B (Figure 9). A constant ratio Li-Si is observed inside all the investigated particles. This ratio varies from a particle to another. Interestingly, as particle 3, some particles investigated were not lithiated at all. Finally, by using AES, we were not able to reveal different phases inside single nanoparticles. However, this technique of surface characterization can be used to study lithium distribution inside the electrode and clearly shows here the heterogeneity of the first lithiation process with different Li concentrations found from one particle to another.

Conclusions

By using XPS and AES, nano silicon based electrodes have been investigated. These techniques of surface characterization are both interesting in two different ways. XPS is relevant to study the SEI and the Si oxides behaviour during cycling. In this work, thanks to XPS analyses, SEI composition on Si anodes has been found to be similar to the composition of the SEI which forms on graphite. The behaviour of the SEI has been observed at different stages of the first electrochemical cycle: (i) the thickness of the SEI is larger for the lithiated electrode and (ii) the composition slightly changes depending on the SOC. Moreover, by using XPS, the evolution of the native oxide layer has been characterized. During the first lithiation, SiO₂ is reduced leading to the formation of a Li_xSiO_y phase and Li₂O. Upon delithiation, Li₂O reacts with Si to form Li_xSiO_y. This reaction is reversible

and happens during the following cycles. Concerning SiO₂, after being reduced, it is not further observed upon cycling. This complete disappearance of the initial oxide layer has not yet been reported in the literature and may have a very strong impact on the cyclability of the electrode. Thus, the conditions to completely reduce SiO₂ after the first cycle such as its initial thickness, the Si morphology, the cycling conditions need to be deeper investigated.

AES allows studying the SEI with respect to its localization at the electrode surface: our results clearly show that, at the end of the first electrochemical cycle, Li is much more abundant at the surface of the conductive agent than that at the surface of silicon. In addition, by combining AES and Ar⁺ sputtering, silicon particles can be investigated individually with respect to their electrode environment and a Li concentration in Si can be determined accurately. Thus, we showed in this work that the first lithiation of electrodes made of nano silicon is a strongly heterogeneous phenomenon with different Li concentrations found in several particles at the electrode surface. We are currently trying to link the particles' electrode environment and this lithium concentration but, undoubtedly, AES already appears as a powerful technique to study and help designing electrodes' architecture.

Acknowledgements

The authors would like to acknowledge the CEA-INSTN for supporting part of this study (PhD funding awarded to Etienne Radvanyi). Surface characterization experiments were performed at the Nanocharacterization Platform, MINATEC Campus, CEA Grenoble.

Notes and references

French Commissary of Atomic and Alternative Energies (CEA), Laboratory of Innovation for New Energy Technologies and Nanomaterials (LITEN), 17 rue des Martyrs, 38054 Grenoble Cedex 9, France. E-mail: severine.jouanneau@cea.fr; Fax: +33 438 784 383; Tel: +33 438 784 034

† Electronic Supplementary Information (ESI) available: Figures S1-S5 corresponding to supplemental electrochemical results, XPS and AES analyses, and SEM images. See DOI: 10.1039/b000000x/

- 1 B. L. Ellis, K. Town and L. F. Nazar, *Electrochim. Acta*, 2012, **84**, 145-154.
- 2 J. B. Goodenough and K.-S. Park, *J. Am. Chem. Soc.*, 2013, **135**, 1167-1176.
- 3 T.-H. Kim, J.-S. Park, S. K. Chang, S. Choi, J. H. Ryu and H.-K. Song, *Adv. Energy Mater.*, 2012, **2**, 860-872.
- 4 D. Larcher, S. Beattie, M. Morcrette, K. Edström, J.-C. Jumas and J.-M. Tarascon, *J. Mater. Chem.*, 2007, **17**, 3759-3772.
- 5 W.-J. Zhang, *J. Power Sources*, 2011, **196**, 13-24.
- 6 M. N. Obrovac and L. Christensen, *Electrochem. Solid-State Lett.*, 2004, **7**, A93-A96.
- 7 L. Y. Beaulieu, T. D. Hatchard, A. Bonakdarpour, M. D. Fleischauer and J. R. Dahn, *J. Electrochem. Soc.*, 2003, **150**, A1457-A1464.
- 8 U. Kasavajjula, C. Wang and A. J. Appleby, *J. Power Sources*, 2007, **163**, 1003-1039.
- 9 J.-I. Lee, J.-H. Park, S.-Y. Lee and S. Park, *Phys. Chem. Chem. Phys.*, 2013, **15**, 7045-7049.
- 10 J. Tu, L. Hu, S. Jiao, J. Hou and H. Zhu, *Phys. Chem. Chem. Phys.*, 2013, DOI: 10.1039/c3cp52777h.
- 11 J. Li, R. B. Lewis and J. R. Dahn, *Electrochem. Solid-State Lett.*, 2007, **10**, A17-A20.

- 12 S. Komaba, N. Yabuuchi, T. Ozeki, Z.-J. Han, K. Shimomura, H. Yui, Y. Katayama and T. Miura, *J. Phys. Chem. C*, 2012, **116**, 1380-1389.
- 13 C. Erk, T. Brezesinski, H. Sommer, R. Schneider and J. Janek, *ACS Appl. Mater. Interfaces*, 2013, **5**, 7299-7307.
- 14 J.-S. Bridel, T. Azais, M. Morcrette, J.-M. Tarascon and D. Larcher, *Chem. Mater.*, 2010, **22**, 1229-1241.
- 15 B. Lestriez, S. Desaever, J. Danet, P. Moreau, D. Plée and D. Guyomard, *Electrochem. Solid-State Lett.*, 2009, **12**, A76-A80.
- 16 H. Wu and Y. Cui, *Nano Today*, 2012, **7**, 414-429.
- 17 P. Gao, H. Jia, J. Yang, Y. Nuli, J. Wang and J. Chen, *Phys. Chem. Chem. Phys.*, 2011, **13**, 20108-20111.
- 18 S. Chen, M. L. Gordin, R. Yi, G. Howlett, H. Sohn and D. Wang, *Phys. Chem. Chem. Phys.*, 2012, **14**, 12741-12745.
- 19 J. Tu, Z. Zhao, L. Hu, S. Jiao, J. Hou and H. Zhu, *Phys. Chem. Chem. Phys.*, 2013, **15**, 10472-10476.
- 20 M. Zhou, F. Pu, Z. Wang, T. Cai, H. Chen, H. Zhang and S. Guan, *Phys. Chem. Chem. Phys.*, 2013, **15**, 11394-11401.
- 21 Y. Oumellal, N. Delpuech, D. Mazouzi, N. Dupré, J. Gaubicher, P. Soudan, B. Lestriez and D. Guyomard, *J. Mater. Chem.*, 2011, **21**, 6201-6208.
- 22 C. Pereira-Nabais, J. Swiatowska, A. Chagnes, F. Ozanam, A. Gohier, P. Tran-Van, C.-S. Cojocar, M. Cassir and P. Marcus, *Appl. Surf. Sci.*, 2013, **266**, 5-16.
- 23 V. Etacheri, Y. Haik, Y. Goffer, G. A. Roberts, I. C. Stephan, R. Fasching and D. Aurbach, *Langmuir*, 2012, **28**, 965-976.
- 24 V. Etacheri, U. Geiger, Y. Goffer, G. A. Roberts, I. C. Stephan, R. Fasching and D. Aurbach, *Langmuir*, 2012, **28**, 6175-6184.
- 25 C. K. Chan, R. Ruffo, S. S. Hong and Y. Cui, *J. Power Sources*, 2009, **189**, 1132-1140.
- 26 B. Philippe, R. Dedryvère, J. Allouche, F. Lindgren, M. Gorgoi, H. Rensmo, D. Gonbeau and K. Edström, *Chem. Mater.*, 2012, **24**, 1107-1115.
- 27 B. Philippe, R. Dedryvère, M. Gorgoi, H. Rensmo, D. Gonbeau and K. Edström, *Chem. Mater.*, 2013, **25**, 394-404.
- 28 C. Pereira-Nabais, J. Swiatowska, A. Chagnes, A. Gohier, S. Zanna, A. Seyeux, P. Tran-Van, C.-S. Cojocar, M. Cassir and P. Marcus, *J. Phys. Chem. C*, 2014, **118**, 2919-2928.
- 29 J. Saint, M. Morcrette, D. Larcher, L. Laffont, S. Beattie, J.-P. Pèrès, D. Talaga, M. Couzi and J.-M. Tarascon, *Adv. Funct. Mater.*, 2007, **17**, 1765-1774.
- 30 Y. M. Lee, J. Y. Lee, H.-T. Shim, J.-K. Lee and J.-K. Park, *J. Electrochem. Soc.*, 2007, **154**, A515-A519.
- 31 B. Guo, J. Shu, Z. Wang, H. Yang, L. Shi, Y. Liu and L. Chen, *Electrochem. Comm.*, 2008, **10**, 1876-1878.
- 32 Q. Sun, B. Zhang and Z.-W. Fu, *Appl. Surf. Sci.*, 2008, **254**, 3774-3779.
- 33 S. Xun, X. Song, L. Wang, M. E. Grass, Z. Liu, V. S. Battaglia and G. Liu, *J. Electrochem. Soc.*, 2011, **158**, A1260-A1266.
- 34 M. T. McDowell, S. W. Lee, I. Ryu, H. Wu, W. D. Nix, J. W. Choi and Y. Cui, *Nano Lett.*, 2011, **11**, 4018-4025.
- 35 K. I. Morigaki and A. Ohta, *J. Power Sources*, 1998, **76**, 159-166.
- 36 Y.-J. Kim, H. Lee and H.-J. Sohn, *Electrochem. Comm.*, 2009, **11**, 2125-2128.
- 37 M. Wu, Z. Wen, Y. Liu, X. Wang and L. Huang, *J. Power Sources*, 2011, **196**, 8091-8097.
- 38 X. Zhou, Y. -X. Yin, L. -J. Wan and Y. -G. Guo, *Adv. Energy Mater.*, 2012, **2**, 1086-1090.
- 39 X. Zhou, L. -J. Wan and Y. -G. Guo, *Adv. Mater.*, 2013, **25**, 2152-2157.
- 40 E. Radvanyi, E. De Vito, W. Porcher, J. Danet, P. Desbois, J.-F. Colin and S. Jouanneau Si Larbi, *S. J. Mater. Chem. A*, 2013, **1**, 4956-4965.
- 41 US patent 5374564 1994.
- 42 M. Gu, Y. Li, X. Li, S. Hu, X. Zhang, W. Xu, S. Thevuthasan, D. R. Baer, J.-G. Zhang, J. Liu and C. Wang, *ACS Nano*, 2012, **6**, 8439-8447.
- 43 Y. Zhu and L. Cao, *Appl. Surf. Sci.*, 1998, **133**, 213-220.
- 44 E. Hüger, L. Dörrer, J. Rahn, T. Panzner, J. Stahn, G. Lilienkamp and H. Schmidt, *Nano Lett.*, 2013, **13**, 1237-1244.
- 45 J. C. Lascovich, R. Giorgi, and S. Scaglione, *Appl. Surf. Sci.*, 1991, **47**, 17-21.
- 46 S. Rey and F. Le Normand, *Thin Solid Films*, 2011, **519**, 4426-4428.
- 47 D. Briggs and J. T. Grant, *Surface Analysis by Auger and X-Ray Photoelectron Spectroscopy*, IM Publications, 2004.
- 48 S. Tanuma, C. J. Powell and D. R. Penn, *Surf. Interface Anal.*, 2004, **36**, 1-14.
- 49 P. B. Balbuena and Y. Wang, *Lithium-Ion Batteries: Solid-Electrolyte Interphase*, Eds, Imperial College Press: London, U.K., 2004.
- 50 R. Younesi, M. Hahlin and K. Edström, *ACS Appl. Mater. Interfaces*, 2013, **5**, 1333-1341.
- 51 K. Kanamura, H. Takezawa, S. Shiraishi and Z.-i. Takehara, *J. Electrochem. Soc.*, 1997, **144**, 1900-1906.
- 52 S. Tanaka, M. Taniguchi and H. Tanigawa, *J. Nucl. Mater.*, 2000, **283-287**, 1405-1408.
- 53 K. W. Schroder, H. Celio, L. J. Webb and K. J. Stevenson, *J. Phys. Chem. C*, 2012, **116**, 19737-19747.
- 54 D. E. Arreaga-Salas, A. K. Sra, K. Roodenko, Y. J. Chabal and C. L. Hinkle, *J. Phys. Chem. C*, 2012, **116**, 9072-9077.
- 55 M. Nie, D. P. Abraham, Y. Chen, A. Bose and B. L. Lucht, *J. Phys. Chem. C*, 2013, **117**, 13403-13412.
- 56 J. Pisonero, N. Bordel and V. S. Smentkowski, *J. Anal. At. Spectrom.*, 2013, **28**, 970-972.
- 57 M. Senoner and W. E. S. Unger, *J. Anal. At. Spectrom.*, 2012, **27**, 1050-1068.
- 58 H. M. Ortner, *J. Anal. At. Spectrom.*, 2007, **22**, 599-607.
- 59 R. Dedryvère, H. Martinez, S. Leroy, D. Lemordant, F. Bonhomme, P. Biensan and D. Gonbeau, *J. Power Sources*, 2007, **174**, 462-468.
- 60 H. Bryngelsson, M. Stjern Dahl, T. Gustafsson and K. Edström, *J. Power Sources*, 2007, **174**, 970-975.
- 61 K. Edström, M. Herstedt and D. P. Abraham, *J. Power Sources*, 2006, **153**, 380-384.
- 62 B. Philippe, R. Dedryvère, M. Gorgoi, H. Rensmo, D. Gonbeau and K. Edström, *J. Am. Chem. Soc.*, 2013, **135**, 9829-9842.
- 63 X.-H. Liu and J. Y. Huang, *Energy Environ. Sci.*, 2011, **4**, 3844-3860.